

## **ScienceDirect**

Procedia CIRP 123 (2024) 322-327



7<sup>th</sup> CIRP Conference on Surface Integrity

# Effect of cutting speed on the surface integrity of single point diamond turned (100)Ge

Michele Tunesi<sup>a</sup>, Eann Lawing<sup>b</sup>, Colton Estes<sup>c</sup>, John Gasson<sup>c</sup>, Brian S. Dutterer<sup>b</sup>, Matthew A. Davies<sup>b,c</sup>, Don A. Lucca<sup>a,\*</sup>

<sup>a</sup>School of Mechanical and Aerospace Engineering, 300 Engineering South, Oklahoma State University, Stillwater, OK, 74078, USA
 <sup>b</sup>Department of Mechanical Engineering, Duke Centennial Hall, University of North Carolina at Charlotte, Charlotte, NC, 28223, USA
 <sup>c</sup>Moore Nanotechnology Systems, 6510 Northpark Blvd, Charlotte, NC, 28216, USA

#### Abstract

The surface integrity of single crystal (100)Ge machined by on-axis single point diamond turning was investigated. The specimen was machined with a -25° rake angle single crystal diamond tool, with a depth of cut of  $10 \mu m$  and a feedrate of  $4 \mu m$ /rev. Six circular bands were machined on the specimen at different cutting speeds, ranging from 0.2 m/s to 10 m/s, while keeping all other machining and geometrical parameters constant. The surface topography was measured by atomic force microscopy and the near surface lattice disorder was investigated by Raman spectroscopy. The cutting and thrust forces were measured during machining, and their frequency domain was analyzed. Machining resulted in four lobes with four-fold symmetry, with differing amounts of surface fracture at each cutting speed. It was found that increasing the cutting speed generates surfaces with less or no brittle fracture for all cutting directions, causing some lobes to be undistinguishable. As the speed increased, the cutting and thrust force decreased monotonically. The frequency content of the force changed accordingly with the appearance of the surface, with a shift from 8 oscillations per revolution to 4 oscillations per revolution.

© 2024 The Authors. Published by Elsevier B.V.
This is an open access article under the CC BY-NC-ND license (https://creativecommons.org/licenses/by-nc-nd/4.0)
Peer-review under responsibility of the scientific committee of the 7th CIRP Conference on Surface Integrity

Keywords: Machining; Single crystal; Cutting speed; Surface topography

## 1. Introduction

Single crystal germanium (Ge) is well suited for the manipulation of infrared (IR) light, due in part, to its high transmittance for wavelengths of 1  $\mu$ m to 12  $\mu$ m [1]. It is currently used in various optical components that include thermal imaging and sensor devices, IR windows, and night vision systems [2]. To reduce the size and weight of optical components, the fabrication of optics with freeform surfaces by single point diamond machining is currently being pursued. Due to its brittle nature, Ge is machined using negative rake angle tools in combination with conservative cutting parameters. This is done to reduce the load applied by the tool on the material, to achieve shear induced plasticity and avoid fracture at the surface. When optimal cutting parameters are chosen, the final topography of the surface is determined by the cutting direction relative to the

crystal direction, as was reported in the seminal turning experiments performed by Nakasuji et al. [3]. It has been previously shown that increasing feedrate when machining (100)Ge with a given rake angle promotes fracture on the surface for all cutting directions [4]. This was also found for (111)Ge, and in addition to increasing the amount of fracture, the elastic modulus of the machined surface was seen to increase with increasing feedrate [5]. When an optimal cutting direction was isolated, the feedrate controlled not only the final surface topography, but also the surface residual stress [6]. In another study it was also found that the topography was insensitive to a range of depths of cut, while the residual stress introduced in the surface depended on the combination of depth of cut and tool rake angle [7]. Until recently, cutting speed was not considered as a parameter that could be varied to improve the surface condition. Recent work has demonstrated that increasing the average cutting speed by two orders of magnitude (from 0.25 m/s to 20 m/s) generated surfaces that had little to no fracture depending on the cutting direction [8]. Counterintuitively, the cutting and thrust forces

<sup>\*</sup> Corresponding author. Tel.: +1 405 744 5899 E-mail address: lucca@okstate.edu

were also seen to decrease monotonically as the cutting speed increased.

In this study, (100)Ge was machined on-axis by single point diamond turning. Six bands were machined with true constant speed and constant feedrate and later analyzed by Raman spectroscopy and atomic force microscopy (AFM). The cutting and thrust forces measured during machining were analyzed, showing the effect of cutting speed on the crystallographic response of the specimen to the cutting direction.

#### 2. Materials and methods

## 2.1. Specimen preparation and machining

A single crystal Ge specimen with a (100) surface orientation was turned on-axis using a Moore Nanotechnology 250 UPL-MP system. A single crystal diamond round nose tool was used to machine the surface. The tool had a 1.008 mm nose radius, a rake angle of -25°, and a clearance angle of 10°. The parameters under experimental control were the depth of cut, spindle rotational speed and the feed velocity, which defined the cutting speed and the feed per revolution.

Cutting and thrust forces were measured during machining by a Kistler MicroDyn dynamometer. The dynamometer's output was amplified and then collected by a NI-DAQ board. To prevent aliasing caused by bandwidth limitations, data acquisition was performed at a frequency of 10 kHz.

Six circular bands were machined on the specimen at different cutting speeds, ranging from 0.2 m/s to 10 m/s. Prior to machining the bands, several cleanup passes were made with a 10  $\mu$ m depth of cut, a feed rate of 0.3  $\mu$ m/rev, and a spindle speed of 2000 RPM. These conservative parameters have been shown to generate a surface with lattice disorder comparable to a surface prepared by chemomechanical polishing [9]. A constant surface speed across a given band was obtained by continuously adjusting the rotational speed of the specimen. The depth of cut was maintained at 10  $\mu$ m, and the feed rate was 4  $\mu$ m/rev. The width of the bands was 2 mm.

## 2.2. Force analysis

Data collection of the cutting and thrust forces began before the engagement of the tool with the specimen and ended several seconds after the tool was disengaged. Due to the machining time the data was corrected for drift in the charge amplifiers used with the piezoelectric dynamometer using the 4 s before and after contact of the tool. This was done by fitting a linear function to the data, and then subtracting it from the dataset using Eq. 1:

$$F'(t) = F(t) - \xi(t) \tag{1}$$

where F'(t) is the corrected dataset, F(t) is the original dataset and  $\xi(t)$  is a linear function with the form  $\xi(t) = mt + q$ . A moving average filter was used to reduce the noise of the dataset.

The moving average function had a time window that was adjusted based on the period of one rotation of the Ge specimen at each cutting speed. The window value was 1/100 of the period. This value was chosen empirically by testing a range of window sizes to determine the size that would reduce the noise without affecting the relative strength of the peaks in the frequency domain. The measured periods of rotation and associated time windows are reported in Table 1. Figure 1 shows an example of the moving average filter applied to the data collected at 0.2 m/s, where noise on the order of 0.1 N was removed. After filtering, the Fast Fourier Transform (FFT) was calculated for both the cutting and thrust forces to evaluate the frequency domain over 100 revolutions of the specimen.

Table 1. Measured period and window size used to filter the data with a moving average function.

Cutting speed [m/s]	Measured period [ms]	Time window [ms]	
0.2	458.3	4.6	
1.3	80.3	0.8	
2	58.3	0.6	
4	32.3	0.3	
8	17.6	0.2	
10	15.2	0.1	

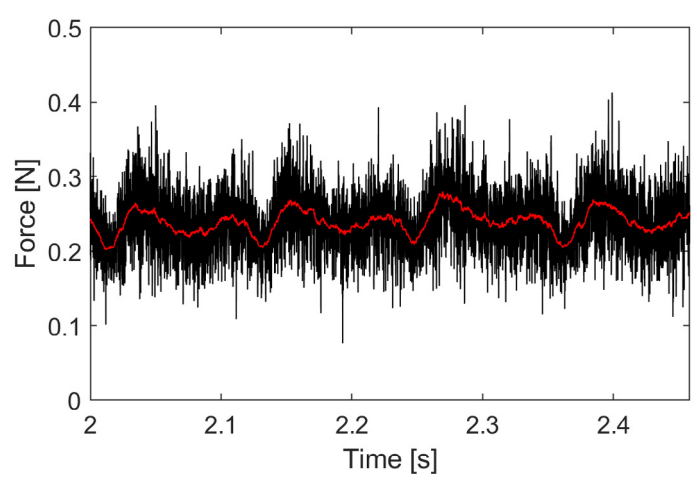


Figure 1. Data of one revolution at 0.2 m/s before (black) and after (red) filtering with a moving average.

#### 3. Results

## 3.1. Surface and subsurface characterization

The (100)Ge specimen exhibited several topography lobes on the surface after machining as shown in Fig. 2a, with a schematic of the appearance of the lobes shown in Fig. 2b. The lobes were regions of similar surface topography that were distributed radially from the center. On each band, they matched the expected 4-fold symmetry of the (100) plane of single crystal Ge. When the cutting speed was 4 m/s or lower, three lobes were visible on the surface. Two of the lobes, defined as the primary and secondary lobes in our previous work [8], had the

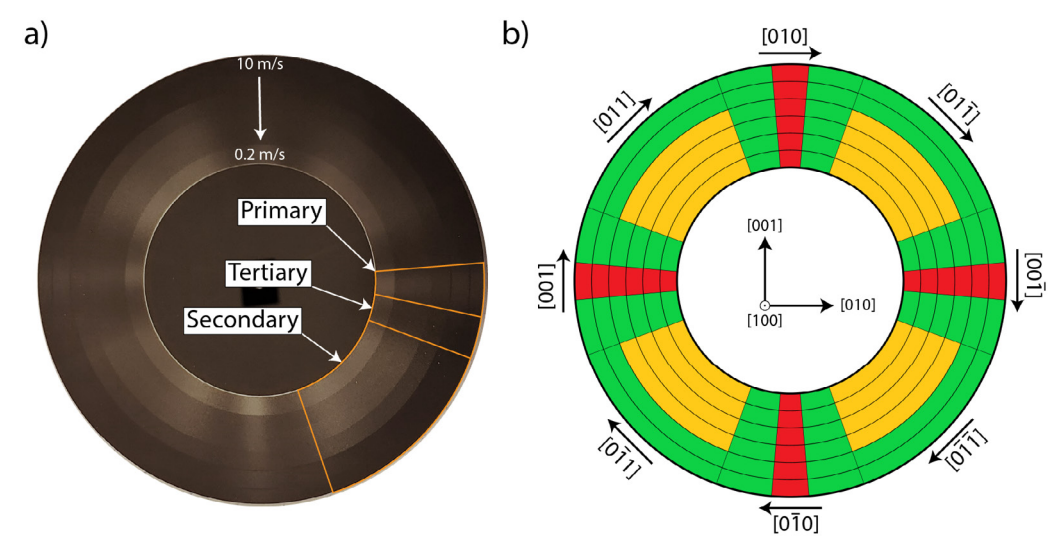


Figure 2. (a) photo of the (100)Ge specimen after machining and (b) schematic of the lobes with similar surface topography.

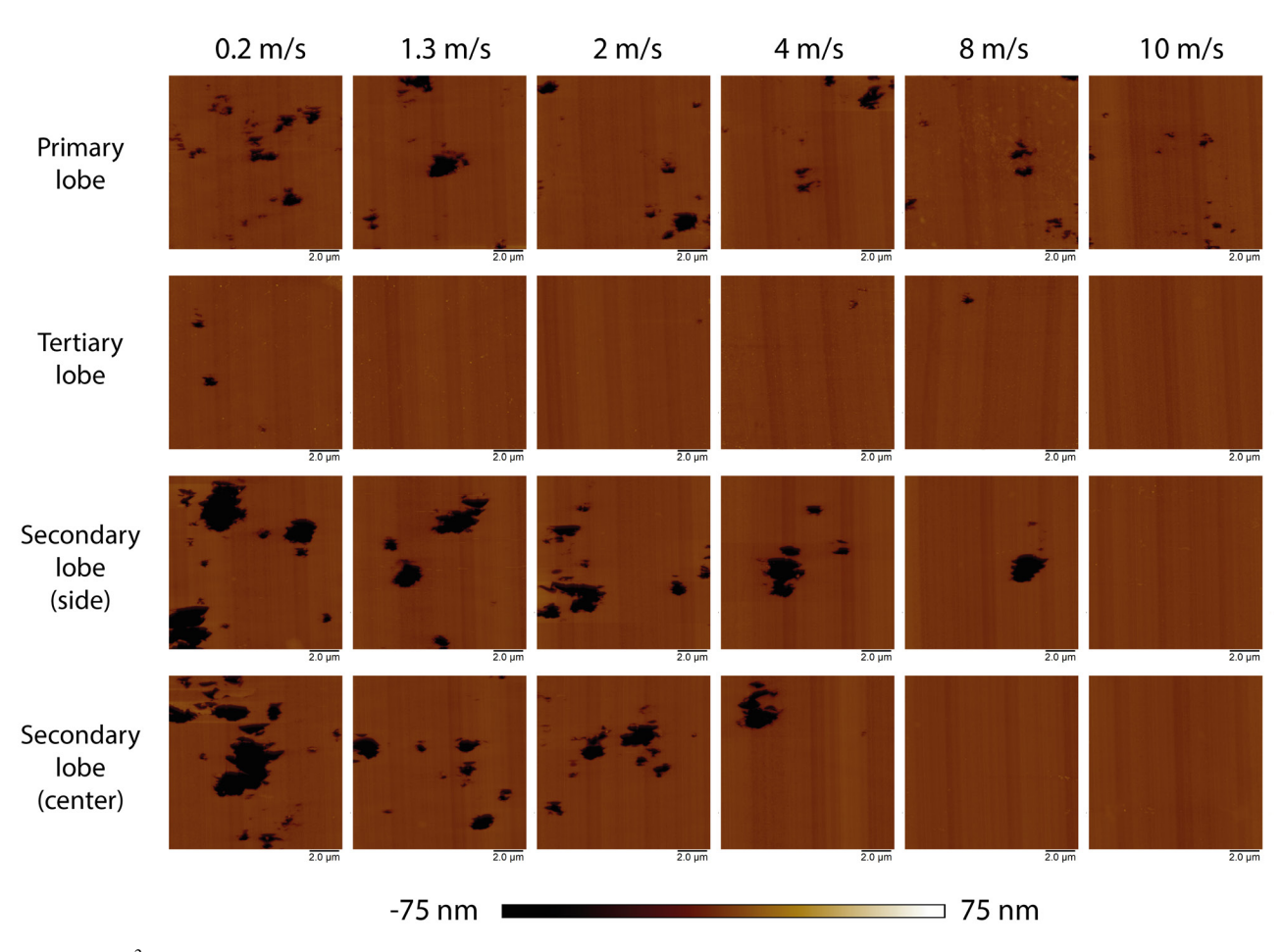


Figure 3.  $10x10 \mu m^2$  AFM measurement on machined (100)Ge at different speeds and for four distinct locations with respect to the four-fold symmetry of the specimen.

most fracture and a hazy appearance. The two lobes are associated with the cutting direction families < 100 > and < 110 > respectively. At the center of the secondary lobe, it appeared that the amount of fracture was lower when compared to the side of the same lobe. As the cutting speed increased, the ap-

pearance of the lobe changed from hazy to specular. A third lobe was present on both sides of the primary lobe, defined as the tertiary lobe, and had a specular appearance for all cutting speeds. Above a cutting speed of 4 m/s, it was not possible to distinguish between the secondary and tertiary lobes.

AFM measurements, shown in Fig. 3, were performed on each band and on four locations: the primary lobe, the secondary lobe (side and center) and the tertiary lobe. The images were obtained using a Bruker AFM operating in tapping mode, and the data was corrected using a flattening filter. The scan size was  $10x10 \mu m^2$ . For all images, the cutting direction was parallel to the vertical direction of the image. The amount and size of the fracture on the surface, represented by the dark regions in the AFM images, decreased with the increase of cutting speed. Considering the primary lobe, fracture was present at all machining conditions, but the severity of the fracture decreased from large pits with a size in the range of 2  $\mu$ m to smaller round pits 100 to 300 nm in size. The secondary lobe did not show a significant difference at lower cutting speed when comparing the center to the side. At higher cutting speed the center of the lobe showed less fracture than the side. The tertiary lobe showed small amounts of fracture and did not change with cutting speed. At 10 m/s the secondary and tertiary lobe were indistinguishable from each other. The resulting fractures did not show any preferred direction with respect to the crystal orientation of the specimen.

Raman spectroscopy was performed in locations comparable to those of the AFM measurements. The shift of the center of the TO (Transverse Optical) Raman mode  $\omega_{TO}$  with respect to 300.7 rel. cm<sup>-1</sup> was calculated by fitting a Lorentzian peak over the measured spectrum and then used to calculate the residual stress with Eq. 2 [10, 11]:

$$P = 0.26\Delta\omega_{TO} = 0.26(\omega_{TO} - 300.7) \tag{2}$$

The bands did not show a difference in surface residual stress where there was no fracture, with an average compressive stress of 0.6 GPa, and when fracture occurred the stress state was neutral. This is shown in Fig. 4, where two Raman areal measurements were performed on the center of the secondary lobe on the bands machined with a cutting speed of 0.2 m/s and 10 m/s. The darker spots in the 0.2 m/s optical image correspond to fracture on the surface. Features parallel to the cutting direction can be distinguished in the Raman data and are associated with peaks and valleys left by the tool. Measurements performed on the chips collected during machining showed a tensile residual stress of 0.7 GPa.

## 3.2. Force analysis

The 4-fold symmetry of the (100) surface was confirmed in the cutting and thrust forces which exhibited 4 or 8 oscillations per period of rotation. The data for one rotation of the specimen at each cutting speed are shown in Fig. 5, where the time for one rotation is the time reported in Table 1. For the lowest cutting speed, there were 8 oscillations per revolution for both the cutting and the thrust force, consistent with the multiple lobes observed. The minimum of the measured forces corresponds to fracture and the primary lobe, while the maximum corresponds to shear-dominated cutting [5]. Eight oscillations are visible also at 1.3 m/s and become less apparent at 2 m/s. When the cutting speed is higher than 2 m/s, the force data shows only 4 oscillations per rotation, consistent with the sec-

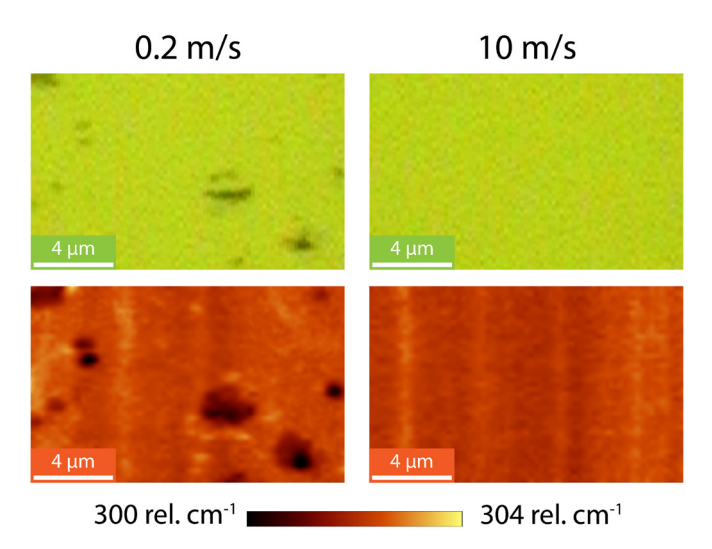


Figure 4. Optical image and center of the TO mode of Ge. The two measurements were performed on the center of the secondary lobe generated with a cutting speed of 0.2 m/s and 10 m/s. The cutting direction is vertical.

ondary and tertiary lobes becoming less distinguishable. Both the maximum and the minimum of all forces decreased monotonically with increasing cutting speed. This result is consistent with our recent work [8]. The minimum and maximum values of the cutting and thrust forces are shown in Fig. 6. The thrust force had a higher noise level compared to the cutting force. Since the thrust force acts normal to the surface, it is expected to be more sensitive to each fracture pit generated on the surface during machining.

The data from 100 revolutions was used to calculate the FFT of the cutting force. Figure 7a shows the frequency domain of each dataset normalized by the rotational frequency,  $\Omega$ , calculated from the inverse of the values shown in Table 1. The intensity was also scaled to have the  $4\Omega$  peak intensity constant for all frequency domains. The frequency domains show a peak at  $\Omega$  which corresponds to the rotational frequency of the specimen during machining. The other major peaks are  $4\Omega$  and its multiples. The intensity of the  $4\Omega$  peak can be explained by the 4-fold symmetry of the (100) plane of Ge. For all cutting speeds, the  $4\Omega$  frequency was one of the most intense. When the  $8\Omega$  frequency is considered, the intensity relative to the  $4\Omega$ decreased with increasing speed, as shown in Fig. 7b. This further confirms that the effect of the secondary lobe measured in the forces at the lowest speeds tends to disappear as the cutting speed increases. This is also true for the higher multiples of  $4\Omega$ .

### 4. Discussion

The decrease of fracture observed with increasing cutting speed indicates a possible shift in material response as the cutting speed is increased. This is supported by the change in topography measured by AFM for all cutting directions. The decrease in the cutting force by 45% also indicates that a more energetically favorable material removal mechanism may dominate. Several mechanisms could contribute to this result, in-

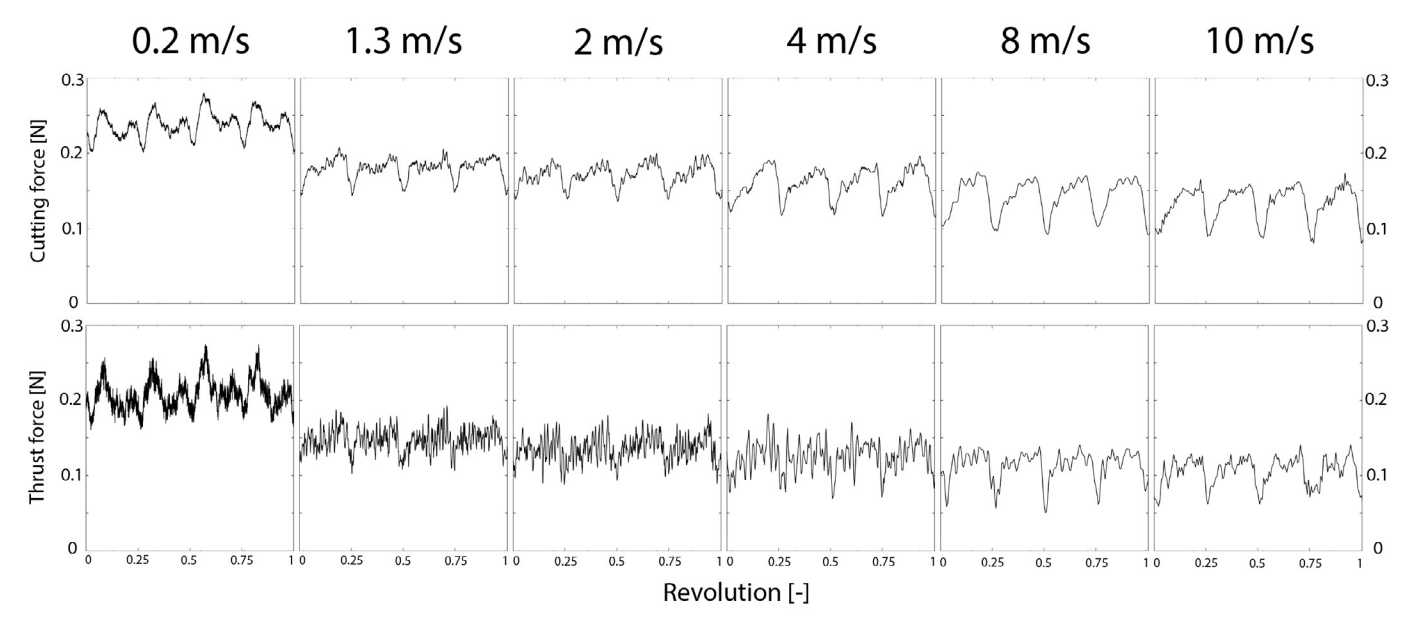


Figure 5. Cutting and thrust forces for one revolution of the specimen. The time for one revolution is listed in Table 1.

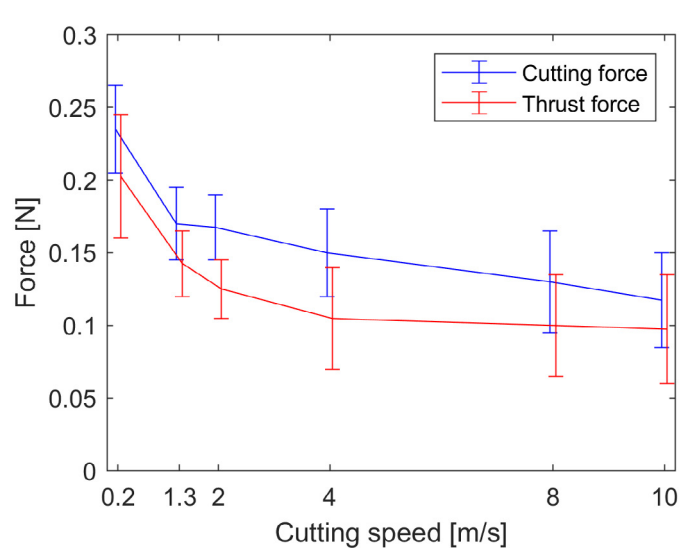


Figure 6. Cutting and thrust force minimum and maximum values measured.

cluding an increased stress state due to inertial effects, strain rate effects including thermal softening, and phase transformation. Single crystal Ge has been shown to undergo a phase transformation from crystalline Ge to  $\beta$ -Sn Ge under a hydrostatic stress of about 10 GPa [12]. The transformation can occur at a stress state as low as 6.7 GPa when shear stress is present [13]. Compared to the crystalline phase, the  $\beta$ -Sn phase has more slip systems available for shearing when being machined [14]. Molecular dynamics simulations predict that this phase transformation could occur during the nanometric cutting of Ge [15]. Using the maximum force measured for both the cutting and thrust force, the resultant force acting at the specimen surface R, and resultant force angle  $\gamma$  can be calculated using Eqs. 3 and 4 respectively.

$$R = \sqrt{F_c^2 + F_t^2} \tag{3}$$

$$\gamma = \tan^{-1}(\frac{F_t}{F_c}) \tag{4}$$

The stress acting at the tool-specimen interface can be estimated using Eq. 5:

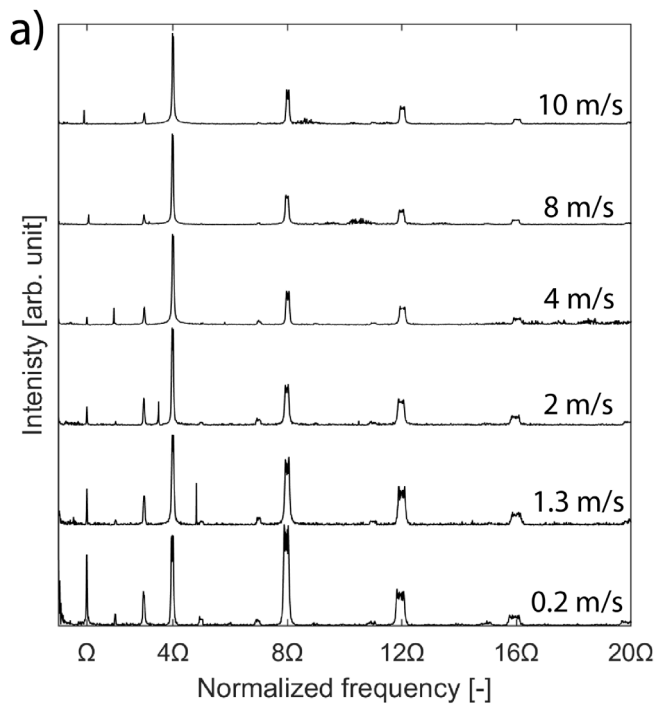
$$\sigma = \frac{R}{A}\cos(|\alpha|)\cos(\gamma - |\alpha|) \tag{5}$$

where R is the resultant force magnitude, A is the cross-sectional area of the chip,  $\gamma$  is the angle between the cutting direction and the resultant force direction and  $\alpha$  is the tool rake angle. Since the feedrate f and the depth of cut  $a_{doc}$  are orders of magnitude smaller than the tool nose radius, A can be approximated by the linear relation  $A = fa_{doc} = 40~\mu m$ . The resultant force, resultant force angle and stress are reported in Table 2. For the lowest cutting speed, the estimated stress normal to the interface results in 7.8 GPa which then decreases as the speed increases.

Table 2. Resultant force, resultant force angle and estimated stress at the toolspecimen interface calculated from the maximum cutting and thrust force.

Cutting speed [m/s]	Resultant force [N]	Resultant force angle [°]	Stress at interface [GPa]
0.2	0.361	43	7.8
1.3	0.255	40	5.6
2	0.239	37	5.4
4	0.228	38	5.1
8	0.213	39	4.7
10	0.202	42	4.4

Cutting speed affects the individual lobes differently. As shown in Figs. 2a and 3, there is almost no difference on the tertiary lobe, while the largest change occurs on the secondary lobe. Current ongoing research on the relation between the resulting stress on the fracture planes and slip systems of single crystal Ge would indicate that the secondary lobe should show



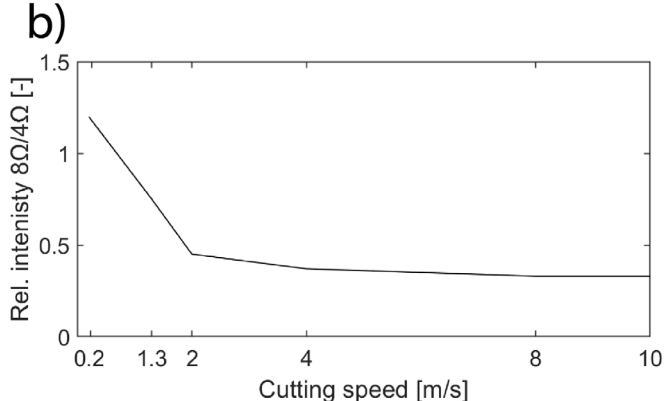


Figure 7. (a) frequency domain of the cutting force normalized by the rotational frequency of the specimen and (b) relative intensity of the  $8\Omega$  frequency peak normalized by the  $4\Omega$  frequency peak.

less fracture before the primary lobe if the slip system of Ge became more energetically favorable.

## 5. Conclusions

Single crystal (100)Ge was single point diamond turned over a range of cutting speeds from 0.2 m/s to 10 m/s. Six circular bands, each produced with different cutting speeds were machined on the specimen while keeping all other machining and geometrical parameters constant. The surface topography measured by atomic force microscopy indicated a reduction in fracture on the surface as the cutting speed increased. For cutting directions belonging to the < 110 > family, as cutting speed increased, apparent fracture disappeared. Accordingly, the secondary lobe that was visible at lower cutting speeds became undistinguishable from the tertiary lobe. Surface residual stresses did not vary with cutting speed. The cutting and thrust forces decreased monotonically as the speed increased and their

frequency content changed from being comprised of 8 oscillations per revolution at 0.2 m/s to 4 oscillations per revolution at 10 m/s. The change in surface topography and the decrease of the forces indicates a possible shift in material response as the cutting speed is increased.

## Acknowledgements

The authors gratefully acknowledge the support of this research by NSF grants CMMI-2210365 and CMMI-2210394.

#### References

- Kaplunov IA, Kolesnikov AI, Kropotov GI, Rogalin VE. Optical properties of single-crystal germanium in the THz range. Opt Spectrosc 2019; 126:191-194.
- [2] Patel M, Karamalidis AK. Germanium: A review of its US demand, uses, resources, chemistry, and separation technologies. Sep Purif Technol 2021;275:118981.
- [3] Nakasuji T, Kodera S, Hara S, Matsunaga H, Ikawa N, Shimada S. Diamond turning of brittle materials for optical components. Cirp Ann 1990; 39(1):89-92.
- [4] Owen JD, Troutman JR, Harriman TA, Zare A, Wang YQ, Lucca DA, Davies MA. The machanics of milling of germanium for IR applications. CIRP Ann 2016; 65(1):109-112.
- [5] Zare A, Tunesi M, Harriman TA, Troutman JR, Davies MA, Lucca DA. Face turning of single crystal (111)Ge: cutting mechanics and surface/subsurface characteristics. J Manuf Sci Eng 2023; 145(7):071007.
- [6] Tunesi M, Lucca DA, Davies MA, Zare A, Gordon MC, Sizemore NE, Wang YQ. Surface integrity of diamond turned (100)Ge. Procedia CIRP 2022; 108:665-669.
- [7] Dutterer BS, Lineberger JL, Smilie PJ, Hildebrand DS, Harriman TA, Davies MA, Suleski TJ, Lucca DA. Diamond milling of an Alvarez lens in germanium. Precis Eng 2014; 38(2):398-408.
- [8] Tunesi M, Sizemore NE, Davies MA, Lucca DA. Effect of cutting speed in single point diamond turning of (100)Ge. Manuf Lett 2023; 38:15-18.
- [9] Sizemore NE. Surface integrity in diamond machining germanium for infrared optics. PhD dissertation, University of North Carolina at Charlotte, 2020
- [10] Olego D, Cardona M. Pressure dependence of Raman phonons of Ge and 3C-SiC. Phys Rev B 1982; 25(2):1151-1160.
- [11] Asaumi K, Minomura S. Effect of pressure on the Raman shift in Ge. J Phys Soc Japan 1978; 45(3):1061-1062.
- [12] Jamieson JC. Crystal structures at high pressures of metallic modifications of silicon and germanium. Science 1963; 139:762-764.
- [13] Qadri SB, Skelton EF, Webb AW. High pressure studies of Ge using synchrotron radiation. J Appl Phys 1983; 54(6):3609-3611.
- [14] Düzgün B, Aytaş I. Investigation of operative slip system in  $\beta$ -Sn single crystal and the relation between the crystal orientation and the slip systems. Jpn J Appl Phys 1993; 32(7):3214-3216.
- [15] Lai M, Zhang X, Fang F, Wang Y, Feng M, Tian W. Study on nanometric cutting of germanium by molecular dynamics simulation. Nanoscale Res Lett 2013; 8:13.